Hindawi
Journal of Nanomaterials
Volume 2017, Article ID 2367856, 15 pages
https://doi.org/10.1155/2017/2367856

Research Article

$CoFe_2O_4$-TiO_2 Hybrid Nanomaterials: Synthesis Approaches Based on the Oil-in-Water Microemulsion Reaction Method

Arturo Adrián Rodríguez-Rodríguez,[1] Sagrario Martínez-Montemayor,[2] César Cutberto Leyva-Porras,[3] Francisco Enrique Longoria-Rodríguez,[1] Eduardo Martínez-Guerra,[1] and Margarita Sánchez-Domínguez[1]

[1]*Centro de Investigación en Materiales Avanzados S. C. (CIMAV) Unidad Monterrey, Alianza Norte 202, Parque de Investigación e Innovación Tecnológica, 66628 Apodaca, NL, Mexico*
[2]*Centro de Investigación en Química Aplicada (CIQA), Blvd. Enrique Reyna Hermosillo 140, 25294 Saltillo, COAH, Mexico*
[3]*Centro de Investigación en Materiales Avanzados, S.C. (CIMAV), Av. Miguel de Cervantes Saavedra 120, Complejo Industrial Chihuahua, 31136 Chihuahua, CHIH, Mexico*

Correspondence should be addressed to Margarita Sánchez-Domínguez; margarita.sanchez@cimav.edu.mx

Received 16 November 2016; Accepted 18 January 2017; Published 8 March 2017

Academic Editor: P. Davide Cozzoli

$CoFe_2O_4$ nanoparticles decorated and wrapped with TiO_2 nanoparticles have been prepared by mixing well-dispersed $CoFe_2O_4$ with amorphous TiO_2 (impregnation approach) and growing amorphous TiO_2 over the magnetic core (seed approach), respectively, followed by thermal treatment to achieve TiO_2 crystallinity. Synthesis strategies were based on the oil-in-water microemulsion reaction method. Thermally treated nanomaterials were characterized in terms of structure, morphology, and composition, to confirm hybrid nanoparticles formation and relate with the synthesis approaches; textural, optical, and magnetic properties were evaluated. X-ray diffraction revealed coexistence of cubic spinel-type $CoFe_2O_4$ and tetragonal anatase TiO_2. Electron microscopy images depicted crystalline nanoparticles (sizes below 25 nm), with homogeneous Ti distribution for the hybrid nanoparticles synthesized by seed approach. EDX microanalysis and ICP-AES corroborated established chemical composition. XPS evidenced chemical states, as well as TiO_2 predominance over $CoFe_2O_4$ surface. According to BET measurements, the hybrid nanoparticles were mesoporous. UV-Vis spectroscopy showed optical response along the UV-visible light region. Magnetic properties suggested the breaking order of magnetic domains due to modification with TiO_2, especially for mediated seed approach sample. The properties of the obtained hybrid nanoparticles were different in comparison with its individual components. The results highlight the usefulness of designed microemulsion approaches for the straightforward synthesis of $CoFe_2O_4$-TiO_2 nanostructured hybrids.

1. Introduction

In the last years, synthesis of nanomaterials has been expanded to the development of more complex structures than single phase nanoparticles (NPs), due to the possibility of coupling a wide range of nanosized building blocks (bounded together by their chemical interfaces) in order to design new materials with enhanced characteristics and improved or innovative properties, combined in one single multifunctional platform [1–4]. These types of nanomaterials are known as hybrid nanoparticles or nanocomposites and emerge as an attractive alternative for technological or scientific applications where conventional NPs cannot compete [5–7]. For instance, in the field of heterogeneous photocatalysis, titanium oxide (TiO_2) based magnetic nanoparticles are used as vehicle for simple and easy separation, from liquid reaction media, by application of an external magnetic field [7–9]. Interestingly, TiO_2 has been one of the most studied semiconductors for photocatalytic applications, standing out due its high photoreactivity, great chemical stability, nontoxicity, and relatively easy and low cost production [10, 11]. Among magnetic components, different spinel-type ferrites (MFe_2O_4, M: divalent metallic ion) have been combined with titanium oxide, to develop highly and

stable magneto-photocatalytic nanocomposites, suitable for the photocatalytic degradation of water pollutants [9, 12–15]. Currently, cobalt ferrite ($CoFe_2O_4$) is a promising candidate for the design of TiO_2 hybrid nanoparticles, owing to its good chemical and thermal stability, and principally magnetic response, moderate magnetic saturation, and low magnetic remanence, ideal for recovery application purposes [16–21]. The proper combination of $CoFe_2O_4$ and TiO_2 has resulted in UV-visible light active nanocomposites (extending the light absorption of titanium oxide), with an improved photocatalytic response in some cases [16, 17, 20]. In light of tailoring the $CoFe_2O_4$-TiO_2 hybrid nanoparticles configuration, the capability of designing complex nanostructures with controlled characteristics (crystallinity, size, surface area, etc.) has been most frequently demonstrated by the combination of two wet chemical methods. For instance, a sol-gel process in reverse microemulsion combined with solvothermal technique [16], coprecipitation/sol-gel [21], hydrothermal/sol-gel [19], and hydrothermal/coprecipitation methods [20]. Other authors have synthesized hybrid $CoFe_2O_4$-TiO_2 system only using one wet chemical route, such as the polymeric precursor method [17], coprecipitation [18], and hydrothermal technique [22]. A great part of these studies carried out the thermal treatment of $CoFe_2O_4$ phase, prior to the integration of titanium oxide, for posterior coupling with TiO_2, and then a second thermal treatment to achieve titanium phase crystallization. The separation of cobalt ferrite from its liquid media increments the possibility of forming bigger $CoFe_2O_4$ agglomerations, decreasing the available surface area to decorate; moreover, it implies more synthesis stages. In this point, the present work proposes a new alternative route for $CoFe_2O_4$-TiO_2 hybrid nanoparticles preparation, through the expansion of the novel oil-in-water (O/W) microemulsion reaction method [23, 24] (reported by our research group), without the necessity of cobalt ferrite prethermal treatment, and adding the benefits of microemulsion synthesis routes. The O/W microemulsion reaction method consists in the use of organometallic precursors, dissolved within nanosized oil droplets (2–50 nm), stabilized by surfactant, and dispersed in a continuous aqueous phase. When a precipitating agent is added, as an aqueous solution directly to the microemulsion without compromising its stability, the reagents will contact each other at the interface, and they will react to form precipitates of nanometric size (NPs); in this context, the water droplets and the interface act as "nanoreactors." The O/W microemulsion method has several advantages; namely, it allows a high control of particle size, a high purity, and good chemical homogeneity under mild conditions. Since water is the continuous and major phase, the method may be considered as more ecologic since the concentration of oil needed is considerably lower and only one microemulsion is needed, instead of two as normally used with the traditional water-in-oil (W/O) microemulsion method [23–25]. Several inorganic nanoparticles have been prepared using the O/W microemulsion method [26–30], including photocatalysts [31, 32] and magnetic nanoparticles [33, 34]. In this sense, the synthesis of the $CoFe_2O_4$-TiO_2 hybrid nanoparticles through the O/W microemulsion method represents a new approach to prepare potential magneto-photocatalytic nanomaterials. Through this study we propose two synthesis strategies; the first one (impregnation approach) consists in the intimate mixing of already formed and crystalline $CoFe_2O_4$ nanoparticles, well-dispersed in oil-in-water microemulsion, with amorphous TiO_2 nanoparticles, obtained, and contained in a microemulsion system with the same oil-surfactant-water composition; the second one is based on a seed mediated approach, where cobalt ferrite (synthesized by the O/W microemulsion method) is employed as nucleation substrate (seed) for the in situ growing of amorphous TiO_2 in a microemulsion reaction system. According to these, two types of hybrid nanoparticles configurations were expected: partial decoration of $CoFe_2O_4$ with TiO_2 and much more uniform wrapping or full coverage of $CoFe_2O_4$ with a TiO_2 nanoparticles layer. The confined self-assembled media at nanoscale, created by the microemulsion environment, may lead to an enhanced synergy between magneto-photocatalytic nanoparticles at their interface, which can result in hybrid $CoFe_2O_4$-TiO_2 nanostructures with good structural characteristics and improved properties. In-depth characterization was performed to evidence $CoFe_2O_4$-TiO_2 hybrid nanoparticles formation, evaluate their properties, and relate obtained characteristics with the developed synthesis approaches.

2. Materials and Methods

2.1. Materials. Iron(III) 2-ethylhexanoate ($C_{24}H_{45}FeO_6$, nominally 50% in mineral spirits) and titanium(IV) 2-ethylhexanoate ($C_{32}H_{60}O_8Ti$, 97%) were purchased from Alfa Aesar. Cobalt(II) 2-ethylhexanoate ($C_{16}H_{30}CoO_4$, 65 wt% solution in mineral spirits), isooctane (C_8H_{18}, CHROMASOLV® Plus for HPLC, ≥99.5%), tetramethylammonium hydroxide pentahydrate TMAH ($C_4H_{13}NO{\cdot}5H_2O$, ≥97%), and ammonium hydroxide NH_4OH (H_5NO, solution 28.0–30.0%) were purchased from Sigma-Aldrich. Synperonic™ 91/5 ($C_{19}O_6H_{40}$) was purchased from CRODA.

2.2. $CoFe_2O_4$-TiO_2 Hybrid Nanoparticles Synthesis. In order to obtain the dual phase nanoparticles, two synthesis approaches were developed. First, we introduce the microemulsions preparation and synthesis of single cobalt ferrite and titanium oxide nanoparticles and then the microemulsion reaction strategies named as "impregnation" and "seed" approaches, based on the synthesis of single $CoFe_2O_4$ and TiO_2 phases. We used a 1 : 3 $CoFe_2O_4$: TiO_2 molar ratio for both cases.

2.2.1. $CoFe_2O_4$ NPs: Microemulsion Preparation and Synthesis. Cobalt ferrite nanoparticles were synthesized by the oil-in-water microemulsion reaction method; for this purpose we formulate a pseudo-ternary system composed of oil (O)/surfactant (S)/deionized water (W) with a 20/20/60 weight percent ratio (wt%). As oil we employed isooctane and as surfactant Synperonic 91/5. The metalorganic precursors iron(III) and cobalt(II) 2-ethylhexanoates (Fe : Co 2 : 1 molar ratio) were previously dissolved in isooctane; Fe and Co were in 0.98 and 1.86 wt% with respect to the nonpolar phase. Constituents were weighted and properly

mixed on a closed vessel and placed in a water bath with controlled temperature. A brown translucent solution (due to precursors coloration) with a low viscosity and lack of birefringence was obtained, in a temperature range from 45 to 55°C. These physical characteristics suggested the formation of an oil-in-water microemulsion, which was confirmed by conductivity measurements (see Supporting Information in Supplementary Material available online at https://doi.org/10.1155/2017/2367856). Below 45°C, a dark-brown and milky mixture was formed, while heating up to 55°C led to phase separation. Once that microemulsion composition and temperature were studied, the confined reaction was carried out at 46°C by adding a 1 M TMAH solution to the microemulsion media, under magnetic stirring until reaching a pH of 12; a dark-brown precipitation evidenced the formation of cobalt ferrite nanoparticles. Stirring and temperature conditions were maintained for 24 hours.

2.2.2. TiO_2 NPs: Microemulsion Preparation and Synthesis. Titanium oxide nanoparticles were also synthesized employing a pseudo-ternary system formulated with a 20/20/60 wt% composition of O/S/W. In this case, titanium(IV) 2-ethylhexanoate was previously dissolved in isooctane, considering 1.19 wt% of Ti with respect to the oil phase. Constituents were weighted and properly mixed on a closed vessel and placed in a water bath with controlled temperature. Using this pseudo-ternary system, we obtained a transparent, fluid, and isotropic liquid solution at a temperature range from 19 to 27°C. Out of this interval, a white milky solution was observed; but interestingly, if temperature was increased from 40 to 43°C a transparent, fluid, and isotropic liquid solution was also obtained. Based on conductivity measurements (Supporting Information), an oil-in-water microemulsion was formed in the 19–27°C range, while a bicontinuous microemulsion was obtained in the 40–43°C range. We decided to carry out the confined reaction at 41°C, due to the proximity to the Co-Fe O/W microemulsion formation. The reaction was conducted by adding NH_4OH concentrate solution (under magnetic stirring) to the Ti colloidal system until reaching a pH of 11; titanium oxide nanoparticles formation was indicated by the formation of a white precipitate. Stirring and temperature conditions were maintained for 24 hours.

2.2.3. $CoFe_2O_4$-TiO_2 Hybrid NPs: Impregnation Approach. Simultaneously, cobalt ferrite and titanium oxide NPs were synthesized in separated vessels, as described. After 24 hours of reaction for $CoFe_2O_4$ NPs, microemulsion temperature was adjusted to 41°C (cobalt ferrite colloidal system was stable at this temperature due to dilution effect through precipitating agent addition); then the TiO_2 NPs microemulsion was poured over cobalt ferrite system under vigorous magnetic stirring. Agitation was maintained for 15 minutes, and then acetone (1/1 ratio in volume) was added to promote $CoFe_2O_4$ impregnation with TiO_2. The color of prepared $CoFe_2O_4$-TiO_2 hybrid nanoparticles was clearly lighter than single $CoFe_2O_4$ nanoparticles, due to the incorporation of titanium oxide phase. Through this approach we expected at least partial $CoFe_2O_4$ NPs decoration with TiO_2 nanoparticles.

2.2.4. $CoFe_2O_4$-TiO_2 Hybrid NPs: Seed Approach. In a first step, $CoFe_2O_4$ NPs were synthesized by the O/W microemulsion method as described; then the required amount of NH_4OH solution for the subsequent titanium oxide precipitation (determined in impregnation approach) was added directly to the cobalt ferrite microemulsion; its temperature was adjusted to 41°C. As a second step, Ti precursor microemulsion was prepared and poured over the $CoFe_2O_4$ nanoparticles microemulsion system. At this stage on its surface, cobalt ferrite is used as nucleation and growing seed for TiO_2 phase. Agitation and temperature conditions were maintained for 24 hours. Similarly, to hybrid nanoparticles prepared by the impregnation approach, the color of as-obtained product was clearly lighter than single $CoFe_2O_4$ nanoparticles. Through this approach, a uniform coating of TiO_2, in the shape of small nanograins, all around $CoFe_2O_4$ surface is attempted.

Both prepared $CoFe_2O_4$-TiO_2 hybrid nanoparticles were separated from their microemulsion media and washed by several cycles of centrifugation (acetone-water mixture, isopropanol, and chloroform) to remove byproducts and impurities. The obtained powders were dried at 70°C and finally thermally treated at 450°C during 5 hours with a heating rate of 5°C/minute under air atmosphere. A $CoFe_2O_4$-TiO_2 NPs physical mixture was also prepared, by mixing (1 : 3 molar ratio) thermally treated cobalt ferrite and thermally treated titanium oxide powders. This sample served as reference material. Figure 1 broadly illustrates the developed synthesis approaches.

2.3. $CoFe_2O_4$-TiO_2 Hybrid NPs Characterization. The crystalline structure of as-synthesized and thermally treated $CoFe_2O_4$-TiO_2 hybrid nanoparticles was determined by X-ray diffraction (XRD) using a PANalytical Empyrean diffractometer, with CuK_α radiation ($\lambda = 0.15418$ nm) at 45 kV and 40 mA. Diffractograms were recorded in the 5–100° range of 2θ, with a step size of 0.0167113° and a time per step of 59.69 s. The morphological characterization was performed by high-resolution transmission electron microscopy in scanning mode (HRTEM-STEM), using a field emission transmission electron microscope, JEM-2200FS (with 0.1 nm resolution) operated at 200 kV. Additionally, energy dispersive X-ray microanalysis (EDX) was carried out, in order to assess the local chemical composition of the nanomaterials. Complementary to this study, inductively coupled plasma atomic emission spectroscopy (ICP-AES) was employed to evaluate the overall chemical composition of the samples, and Thermo Jarrell Ash iCAP 6000 equipment was used. On the other hand, the textural properties of the thermally treated hybrid NPs were determined by nitrogen adsorption-desorption isotherms (at 77 K), employing an automatic Quantachrome Autosorb instrument; prior to the N_2 adsorption, all the samples were outgassed at 150°C for 3 hours. Surface area and the mean pore size diameter were calculated using the Brunauer-Emmet-Teller (BET) and Barrett-Joyner-Halenda (BJH) methods, respectively. The optical properties were determined by diffuse reflectance (DR) UV-Vis measurements, using UV-Vis-NIR spectrophotometer from Agilent Technologies, with an integrating sphere configuration; the

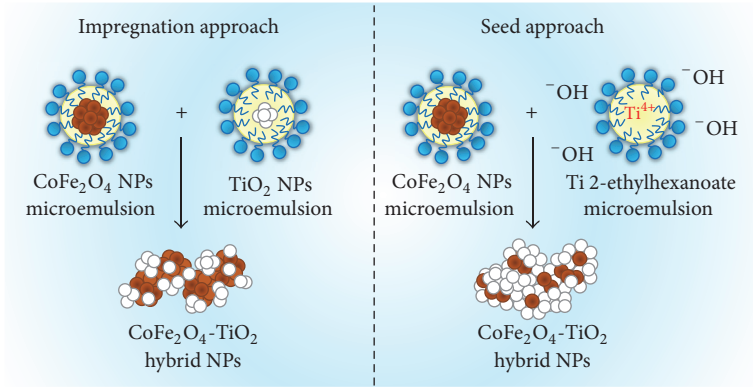

Figure 1: Diagram of impregnation and seed hybrid $CoFe_2O_4$-TiO_2 NPs synthesis approaches, based on O/W microemulsion reaction method.

DR UV-Vis spectra were acquired in the 200–1000 nm range. The magnetic properties of thermally treated cobalt ferrite and $CoFe_2O_4$-TiO_2 hybrid nanoparticles were recorded at 300 K using a vibrating sample magnetometer (quantum design PPMS with VSM option) with a maximum magnetic field of ±60,000 Oe. The chemical surface composition was studied by X-ray photoelectron spectroscopy (XPS), analyses were carried out by means of a Thermo Scientific Escalab 250 Xi instrument, with a working pressure of ~10^{-10} mbar, and the photoelectrons were generated with an AlKα (1486.68 eV) source. The X-ray voltage and power were 14 kV and 350 W, respectively. The spectra were obtained using a pass energy of 50 eV. Peak fitting with Voight profiles was performed using the Thermo Avantage software V 5.41. The baseline corrections were made using the Shirley-Sherwood method. Binding energies were referenced to the C (1s) peak fixed at 284.8 eV.

3. Results and Discussion

3.1. $CoFe_2O_4$-TiO_2 Hybrid Nanoparticle Synthesis. The mechanism of $CoFe_2O_4$-TiO_2 hybrid nanoparticles formation can be explained by means of the oil-in-water microemulsion reaction principles [23, 24]. For $CoFe_2O_4$ synthesis, the Fe(III) and Co(II) 2-ethylhexanoates were contained in nanosized isooctane droplets, stabilized by a monolayer of hydrophilic Synperonic 91/5 surfactant, and dispersed in a continuous aqueous phase. After the addition of a water soluble base, as TMAH (a source of OH^- species), a precipitation reaction occurs (presumably through the oil/water interface), leading to the formation of an iron-cobalt oxide, inside the oil droplets that act as nanoreactors, confining the formed compound at the nanoscale level. Once the first inorganic nuclei were formed and after 24 hours of reaction, the $CoFe_2O_4$ cubic-spinel phase is formed and dispersed in the colloidal system, at the adequate temperature conditions. After cobalt ferrite formation, the two planed strategies (impregnation and seed) were followed, using $CoFe_2O_4$ NPs as substrates, attempting to attach the titanium oxide on its surface. By the impregnation approach, the cobalt ferrite is mixed with already formed amorphous TiO_2 NPs, which were also obtained by a microemulsion reaction process. Assuming the small size of microemulsion droplets as well as obtained products and the huge oil/water interfacial area, there must be a great level of interaction at the nanoscale level between the inorganic phases, leading to a good distribution of titanium oxide-cobalt ferrite nanoparticles. After the destabilization of the resulting colloidal system (through acetone addition), the coagulation of the nanoparticles must promote intimate incorporation of TiO_2 amorphous nanoparticles over the cobalt ferrite system. On the other hand, by the seed approach, the first nuclei of amorphous TiO_2 must grow directly on cobalt ferrite surface nanoparticles, due to the in situ confined reaction of Ti(IV) 2-ethylhexanoate, driven by the collisions amongst oil droplets (containing $CoFe_2O_4$ NPs) and the oil/water interface reaction with unreacted NH_4OH, contained in the aqueous phase of $CoFe_2O_4$ NPs microemulsion. This strategy must produce a more efficient coating over cobalt ferrite nanoparticles than the impregnation approach. Finally the thermal treatment of both synthesized heterostructures led to the decomposition of organic byproducts and complete crystallization of inorganic phases.

3.2. $CoFe_2O_4$-TiO_2 Hybrid NPs Characterization

3.2.1. X-Ray Diffraction. Figure 2 shows the XRD patterns of as-obtained $CoFe_2O_4$ and TiO_2 single NPs and $CoFe_2O_4$-TiO_2 hybrid nanoparticles synthesized by impregnation and seed approaches, before thermal treatment. As it can be seen, as-obtained $CoFe_2O_4$ pattern corresponds to a polycrystalline material, whose signals (∗) at 2θ = 18.50°, 30.46°, 35.95°, 43.60°, 57.52°, and 63.18° can be assigned to the (111), (220), (311), (400), (511), and (440) crystalline planes of cubic spinel-type cobalt ferrite (JCPDS 04-006-4150). On the other hand, as-obtained titanium oxide pattern showed well broadened peaks indicating that the prepared phase is amorphous. Results in Figure 2 coherently show that as-obtained $CoFe_2O_4$-TiO_2 hybrid nanoparticles barely exhibit the crystalline planes related to the cobalt ferrite phase (∗), as shown in the corresponding XRD patterns. The broadened profile and poor intensity of these

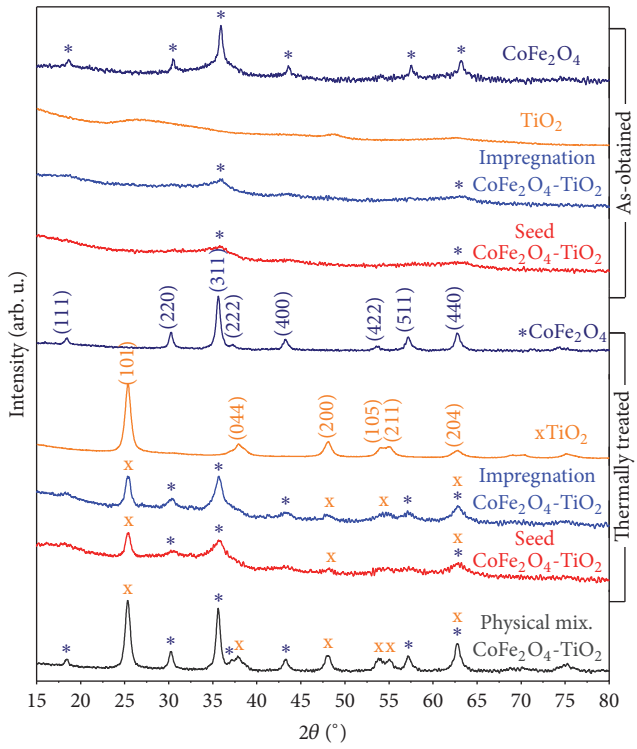

FIGURE 2: X-ray diffraction patterns of synthesized single NPs and hybrid $CoFe_2O_4$-TiO_2 nanoparticles before (as-obtained) and after thermal treatment.

signals are consequence of the amorphous TiO_2 and the nanosized $CoFe_2O_4$. These results confirm the capacity of the O/W microemulsion method to produce structures with certain crystallinity under mild conditions, in our case at least for the single cobalt ferrite phase when using TMAH 1 M as precipitating agent, in contrast to other synthesis methods where thermal treatment is needed to produce crystalline $CoFe_2O_4$ [35–40], even if compared with some water-in-oil microemulsion synthesis methods [41, 42]. Otherwise, the lack of long-range ordering for as-obtained TiO_2 is a common feature at mild conditions as reported [24, 31]. In the same figure, XRD patterns of thermally treated samples are presented. The corresponding cobalt ferrite pattern presents more defined peaks, revealing an improved crystallinity as a result of the atomic ordering promoted by the heating stage. However, the effect of thermal treatment is more evident in the pattern of the thermally treated titanium oxide, in contrast with as-obtained TiO_2. The related XRD profile exhibits peaks (x) at $2\theta = 25.38^\circ$, 37.84°, 48.10°, 53.96°, 55.17°, and 62.81° that are in good agreement with the (101), (044), (200), (105), (211), and (204) crystalline planes of the TiO_2 in the tetragonal phase known as anatase (JCPDS 04-002-8296), the most photocatalytic active TiO_2 phase according to literature [43, 44], without evidence of other titanium polymorphs. In order to understand the diffraction effect of the crystalline TiO_2 contribution to the cobalt ferrite phase and the influence of the synthesis approach, the reference $CoFe_2O_4$-TiO_2 NPs physical mixture was analyzed. The resulting pattern is a simple sum of the diffraction from cubic spinel-type $CoFe_2O_4$ and tetragonal anatase TiO_2 which is evident if compared with corresponding XRD profiles (thermally treated $CoFe_2O_4$ and TiO_2). In the XRD profiles of thermally treated $CoFe_2O_4$-TiO_2 hybrid nanoparticles, obtained by the impregnation and seed approaches, it is possible to observe similarities with the $CoFe_2O_4$-TiO_2 NPs physical mixture. At least the three main reflections from each crystalline phase ($CoFe_2O_4$ (∗): (220), (311), and (440); TiO_2 (x): (101), (200), and (204)) appear in the thermally treated hybrid nanoparticles. This fact makes sense due to the nanosized character of samples with intrinsic broadening and poor peaks. This condition limits the possibility of observing minor intensity peaks. Thermal treatment improves crystallinity evidenced through the higher intensity if compared with as-obtained samples; however this crystallinity is lower if compared with XRD profile from $CoFe_2O_4$-TiO_2 NPs physical mixture; the lower intensity of diffraction signals has also been reported for the coating of a magnetic phase with TiO_2 nanoparticles [45], although not at the same proportion compared to this work. If $CoFe_2O_4$-TiO_2 XRD profiles are compared from impregnation and seed approaches we found a difference. For instance, the thermally treated $CoFe_2O_4$-TiO_2 hybrid nanoparticles obtained by impregnation approach present a more defined $(311)_{CoFe_2O_4}$ reflection. This result could be due to the fact that TiO_2 nanocrystals are not completely wrapping the cobalt ferrite phase. In the case of the thermally treated $CoFe_2O_4$-TiO_2 hybrid NPs obtained by seed approach, a less defined $(311)_{CoFe_2O_4}$ reflection is observed, surely due to a more intimate wrapping of $CoFe_2O_4$ phase within TiO_2 nanocrystals, as a consequence of the titanium in situ reaction carried out over cobalt ferrite seeds. The mixing of already formed $CoFe_2O_4$ and TiO_2 NPs, dispersed in microemulsions as in the impregnation synthesis approach, results in a better strategy to obtain a more uniform wrapping of cobalt ferrite with TiO_2, if it is compared with the simple NPs physical mixture, but less effective if it is compared with the seed approach. The crystallite mean size (d_{XRD}) of $CoFe_2O_4$ and TiO_2 on thermally treated samples was estimated by Rietveld refinement (Table 1), and instrumental contribution using a CeO_2 NIST reference standard (Code SRM 674b) was previously determined in order to assess d_{XRD} values; related cell parameters were also estimated and reported in Table 1.

As it can be seen, the seed synthesis approach yielded a smaller $CoFe_2O_4$ crystallite mean size than impregnation approach; this can be attributed to a growing inhibition effect (even after thermal treatment), caused by the uniform TiO_2 wrapping over cobalt ferrite surface. Meanwhile, the TiO_2 crystallite mean size estimated for the seed sample is slightly larger than that obtained for the impregnation approach; thus it is possible to assume that titanium oxide crystallization is not as affected as for supporting ferrite, under the decoration process and the applied thermal treatment carried out by the synthesis approaches. In the case of $CoFe_2O_4$-TiO_2 NPs physical mixture, it is evident that crystallite mean sizes for $CoFe_2O_4$ and TiO_2 phases are almost the same compared to the corresponding single nanoparticles; these results are coherent since this sample is powder-powder mixing of

Table 1: Crystallite mean size (d_{XRD}) and cell parameters of thermally treated single NPs and hybrid $CoFe_2O_4$-TiO_2 nanoparticles (impregnation (I) and seed (S) approaches); single NPs physical mixture (PM).

Sample ID	$CoFe_2O_4$		TiO_2			$\alpha = \beta = \gamma$ (°)	R Bragg
	d_{XRD} (nm)	a (Å)	d_{XRD} (nm)	a (Å)	c (Å)		
$CoFe_2O_4$	19.08	8.374	—	—	—	90	0.56
TiO_2	—	—	12.81	3.786	9.488	90	1.64
I $CoFe_2O_4$-TiO_2	7.34	8.369	15.6	3.79	9.488	90	0.51
S $CoFe_2O_4$-TiO_2	3.17	8.384	17.45	3.782	9.507	90	0.65
PM $CoFe_2O_4$-TiO_2	17.54	8.368	13.86	3.789	9.502	90	0.49

magneto-photocatalytic phases. In regard to estimated cell parameters, it is possible to observe deviations from the cubic spinel structure cell parameters, for $CoFe_2O_4$, and from the tetragonal structure cell parameters, for anatase TiO_2. These deviations can be explained by the probable substitution of Fe^{3+} (0.64 Å) and/or Co^{2+} (0.65 Å) for Ti^{4+} ions (0.68 Å) into the tetragonal lattice structure of anatase TiO_2 as a consequence of their similar ion sizes, due to ion diffusion (at the interfaces) because of thermal treatment conditions, as similarly reported by Raju and Murthy [46]. However, the absence of extra peaks in the XRD patterns and thus the lack of secondary phases confirm that not solid reaction occurred between cobalt ferrite and titanium oxide NPs. Finally, it is worth mentioning that the thermal treatment temperature (450°C) was established taking into consideration the fact that for temperatures above 550°C iron diffusion into the TiO_2 layer may occur, forming Fe_2TiO_5 (PDF #01-070-2728) as a secondary phase (Supporting Information); this commonly happens with Fe rich compositions in the presence of titania, as reported by Gao et al. for the synthesis of TiO_2/γ-Fe_2O_3 [47]. Moreover, the thermal treatment time was chosen taking into account the fact that TiO_2 crystallization in the $CoFe_2O_4$-TiO_2 hybrid nanoparticles did not occur at the same rate compared to pure TiO_2; hence, in order to achieve a higher crystallinity we extend the thermal treatment of the materials for 5 hours, as shown in the XRD patterns. The delay of TiO_2 crystallization could be related to the nanosized character of hybrid NPs after thermal treatment. Probably, intimate wrapping between $CoFe_2O_4$ and TiO_2 nanocrystals and a higher melting point for nanostructures could control in some ways the intrinsic diffusion processes.

3.2.2. High Resolution Electron Transmission Microscopy-STEM Mode and EDX Analysis/ICP-Atomic Emission Spectroscopy Analysis. Figure 3 presents representative bright field HRTEM-STEM electron micrographs of thermally treated samples: cobalt ferrite, titanium oxide single nanoparticles, and $CoFe_2O_4$-TiO_2 hybrid nanoparticles, prepared by impregnation and seed approaches. First, $CoFe_2O_4$ analyzed zone depicts agglomerated nanoparticles, with a semiglobular morphology and sizes below 25 nm; similarly, TiO_2 exhibits agglomerated nanoparticles but with smaller sizes, below 15 nm, and also semiglobular morphology. As it can be seen, the corresponding inset images display the presence of nanocrystals, as denoted by their lattice fringes, making evident the crystallinity of $CoFe_2O_4$ and TiO_2 nanoparticles. The measured interplanar spacings are in good accordance with cubic-spinel phase of cobalt ferrite and anatase phase of titanium oxide. In the same figure, bright field micrographs of synthesized hybrid nanoparticles (impregnation and seed approaches) depict nanostructured materials apparently composed of smaller nanoparticles, in comparison with bare cobalt ferrite, due to the surface integration of titanium oxide over cobalt ferrite NPs surface. According to Fu et al., who synthesized core-shell $CoFe_2O_4$-TiO_2 heterostructures by coprecipitation/sol-gel route, cobalt ferrite nanoparticles must absorb electrons more strongly than TiO_2 (because $CoFe_2O_4$ possess a higher atomic number); consequently darker regions on electron micrographs could be assigned to Co-Fe phase [21]; however, in our case obtained nanoparticles are much smaller and tend to form agglomerates (thus thicker regions), which provides also image contrast, as shown in single nanoparticles images, making it difficult to carry out a proper identification of the magnetic and photocatalytic components at view. Moreover, through titanium oxide modification, the ferrite nanoparticles show diffuse boundaries, as similarly reported by Stefan et al. [4] for core-shell Fe_3O_4-TiO_2 nanoparticles of sizes below 20 nm. In order to assess the distribution of Fe, Co, and Ti, on the hybrid $CoFe_2O_4$-TiO_2 nanoparticles, an elemental mapping was performed; corresponding images are exhibited in Figure 3. As expected, the impregnation synthesis approach led to a less uniform elemental distribution, compared to the hybrid NPs synthesized by seed approach, that assures a more intimate coupling with titanium oxide phase. Related semiquantitative analysis by EDX is shown in Table 2, and it is evident that there is a deviation from the expected nominal values; nonetheless obtained Co : Fe ratio is close to the 1 : 2 stoichiometry ($CoFe_2O_4$). In the case of Ti, the experimental value is higher; this could be attributed to the wrapping of titanium oxide over cobalt ferrite surface that partially screened the signals of cobalt and iron. Complementary to this study, ICP-atomic emission spectroscopy analysis of the samples is also shown in Table 2; as it can be seen, the overall experimental composition is very close to the $CoFe_2O_4$-TiO_2 nominal values; thus it is possible to affirm that the microemulsion synthesis method conducted to a well-defined chemical composition. On the other hand, Figure 4 presents higher magnification electron micrographs of hybrid nanoparticles. As observed, the images also display the presence of nanocrystals. Fast Fourier transformation was applied in the highlighted zones (using *Digital Micrograph* software), with the aim of obtaining the corresponding electron diffraction patterns (EDPs). For the EDPs from the impregnation hybrid nanoparticles, the

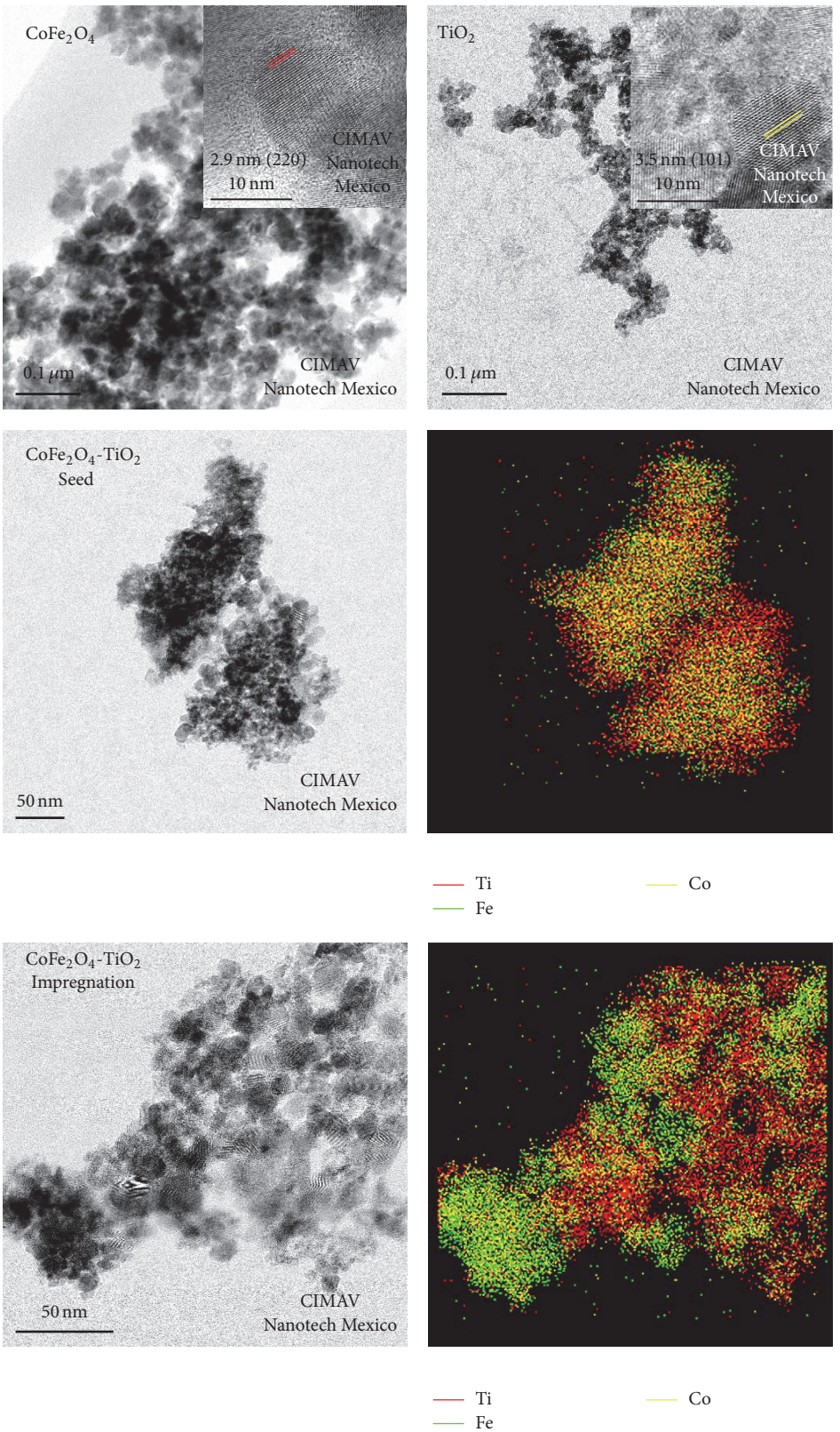

Figure 3: HRTEM-STEM bright field micrographs of thermally treated single nanoparticles: cobalt ferrite and titanium oxide, and thermally treated hybrid $CoFe_2O_4$-TiO_2 NPs, synthesized by seed and impregnation approaches. Elemental mapping images of hybrid NPs are also annexed.

Table 2: Semiquantitative and quantitative chemical analysis by EDX and ICP-AES, respectively, of thermally treated $CoFe_2O_4$-TiO_2 hybrid nanoparticles, synthesized by the impregnation and seed microemulsion approaches.

Hybrid $CoFe_2O_4$-TiO_2 NPs		EDX analysis		ICP-AES	
Element	Nominal ratio	Impregnation	Seed	Impregnation	Seed
Co	1	0.45	0.72	1.030	1.070
Fe	2	1.12	1.34	2.018	1.855
Ti	3	3.39	2.68	2.795	2.789

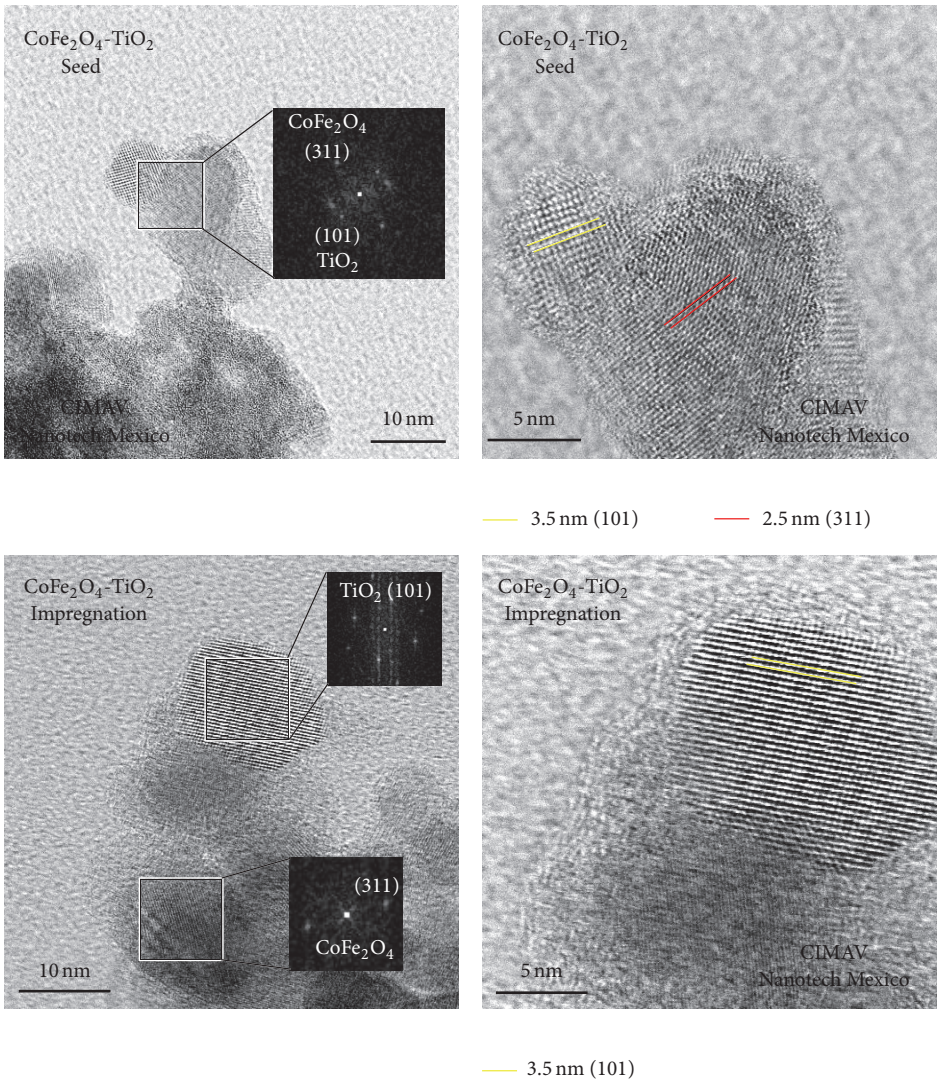

Figure 4: HRTEM-STEM bright field micrographs (higher magnification) of thermally treated hybrid $CoFe_2O_4$-TiO_2 nanoparticles.

calculated *d*-spacings ~2.5 and ~3.5 Å are in agreement with (*hkl*) (311) and (101) interplanar distances of the cubic spinel-type $CoFe_2O_4$ (JCPDS 04-006-4150) and the anatase TiO_2 (JCPDS 04-002-8296), respectively. In accordance with the impregnation microemulsion synthesis approach, the image of the hybrid nanoparticles displays an apparently random distribution of $CoFe_2O_4$ and TiO_2 nanocrystals, as a result of the microemulsion-microemulsion mixing of $CoFe_2O_4$ with amorphous TiO_2 nanoparticles, and the posterior thermal treatment. Otherwise, for the EDPs from the seed hybrid nanoparticles, the calculated *d*-spacings ~2.5 and ~3.5 Å are in agreement with (*hkl*) (311) and (101) interplanar distances of the $CoFe_2O_4$ and TiO_2. In accordance with the seed approach, the image of the hybrid nanoparticles exhibits a TiO_2 nanocrystal jointed directly on the surface of a cobalt ferrite nanocrystal, in addition to a wrapping that could be associated with the titania phase, as a result of the in situ reaction of Ti precursor over the $CoFe_2O_4$ nanocrystals used as a seed. In general, the HRTEM-STEM results confirm the coexistence of $CoFe_2O_4$ and TiO_2 in one platform

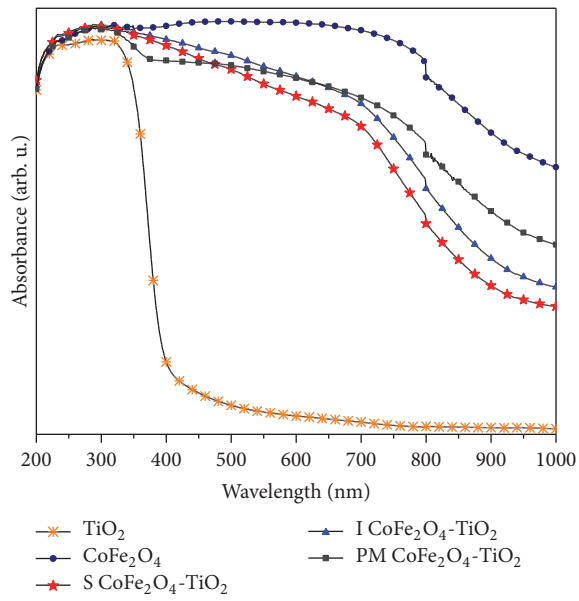

Figure 5: Diffuse reflectance UV-Vis absorption spectra of thermally treated samples: single $CoFe_2O_4$ and TiO_2 nanoparticles and hybrid $CoFe_2O_4$-TiO_2 nanoparticles synthesized by the (I) impregnation and (S) seed approaches. NPs physical mixture (PM) is also presented.

and therefore the achievement of the $CoFe_2O_4$-TiO_2 hybrid nanoparticles by the two planned synthesis approaches. As demonstrated, the characteristics of the hybrid nanoparticles are dependent on the synthesis approach.

3.2.3. Optical Properties. In Figure 5 UV-Vis diffuse reflectance spectra of thermally treated samples, single $CoFe_2O_4$ and TiO_2 and hybrid $CoFe_2O_4$-TiO_2 nanoparticles, are presented. As evident, TiO_2 is absorbed strongly in the UV region, below a band edge of ~400 nm, whereas the optical absorption of $CoFe_2O_4$ spreads along the UV-visible spectrum, decreasing near the infrared region. Similarly, a broad absorption starting from UV and extended to the visible light region is evident from the spectra of hybrid $CoFe_2O_4$-TiO_2 nanoparticles prepared by the seed approach, indicating a red shift compared with pure TiO_2, as a result of the coupling with cobalt ferrite phase. According to similar works, the increasing of TiO_2 optical absorption is attributed to the substitution of Fe^{3+} (0.64 Å) and/or Co^{2+} (0.65 Å) for some Ti^{4+} (0.68 Å) ions in the titanium oxide lattice structure, as shown previously from the calculation of $CoFe_2O_4$ and TiO_2 parameter cells. This ion substitution implies a change into the TiO_2 electronic structure, and the Fe^{3+}/Co^{2+} modification acts as a new impurity level between the valence or conduction band, narrowing the original bandgap, and enhancing the visible light absorption response [18, 20, 48]. In the same way, the optical response of the thermally treated hybrid nanoparticles prepared by the impregnation approach is favored to the visible light, and although the spectra of both hybrids are overlapped at the ~200–350 region, it is possible to notice that impregnation hybrid nanoparticles exhibit a slight band edge displacement to the near infrared region, in addition to a small increment in absorption intensity. These differences are a consequence of their peculiar structural characteristics; for instance, the impregnation sample has not the same arrangement of TiO_2 nanocrystals if compared with the material synthesized by the seed approach (as demonstrated by HRTEM-STEM results); however, both materials are well coupled. This fact is more evident if we compare the hybrid nanoparticles spectra against the spectra of the NPs physical mixture, as it can be seen the $CoFe_2O_4$-TiO_2 physical mixture spectra clearly exhibit a decay in absorbance below 450 nm, the band edge absorption of pure TiO_2, in contrast with hybrid nanoparticles whose titania band edge absorption is apparently modified due to the strong interaction between inorganic phases.

Taking into consideration the optical response showed by the hybrid $CoFe_2O_4$-TiO_2 nanoparticles, it is possible to affirm that the synthesized nanomaterials meet the optical requirements to be active under ultraviolet and/or visible light illumination, in contrast with single TiO_2 nanoparticles.

3.2.4. Textural Properties. Nitrogen adsorption/desorption isotherms curves (at 77 K) of thermally treated samples, single $CoFe_2O_4$ and TiO_2 nanoparticles and hybrid $CoFe_2O_4$-TiO_2 nanoparticles, are exhibited in Figure 6. It is well known that the shape of the adsorption/desorption isotherm is related to the texture of the solid. In this sense, TiO_2 nanoparticles depict a type IV isotherm and an H-2 hysteresis loop, in the relative pressure range of 0.5–1 [44, 49, 50]. This fact implies that thermally threated TiO_2 is presumably mesoporous (pore sizes between 2 and 50 nm), as estimated by a pore size distribution centered at 14.8 nm and a pore volume of 1.6 cm^3/g, employing the BJH (Barrett-Joyner-Halenda) method. Moreover, the specific surface area of TiO_2 was calculated using the BET (Brunauer-Emmett-Teller) method, obtaining a value of 403 m^2/g. In the case of the $CoFe_2O_4$ nanoparticles isotherm curve, it is evident that the amount of N_2 being adsorbed (as function of the relative pressure) is much lower than pure TiO_2, mainly due to the inherent nonporous character of cobalt ferrite [51] compared with titanium oxide. On the other hand the $CoFe_2O_4$-TiO_2 hybrid nanoparticles isotherms display wider hysteresis loops at a high relative pressure, compared with pure $CoFe_2O_4$, indicating also a larger volume of gas being adsorbed. The profiles of the corresponding curves exhibit a mesoporous behavior due to the integration of titanium oxide phase; however, from calculated textural properties (Table 3), it is clear that thermally treated $CoFe_2O_4$-TiO_2 samples possess surface area values closer to the values presented by cobalt ferrite phase. Thus the textural properties of the hybrid $CoFe_2O_4$-TiO_2 nanoparticles are likely due to the combination of inherent porosity and the interparticle arrangement, achieved from the packing of neighbouring nanoparticles. The reported surfaces areas of microemulsion prepared hybrid $CoFe_2O_4$-TiO_2 nanoparticles are higher to the value reported for $CoFe_2O_4$-TiO_2 nanomaterials synthesized by methods such as the polymeric precursor method (75.29 m^2/g) [17], with a $CoFe_2O_4$: TiO_2 weight ratio of 56 : 44.

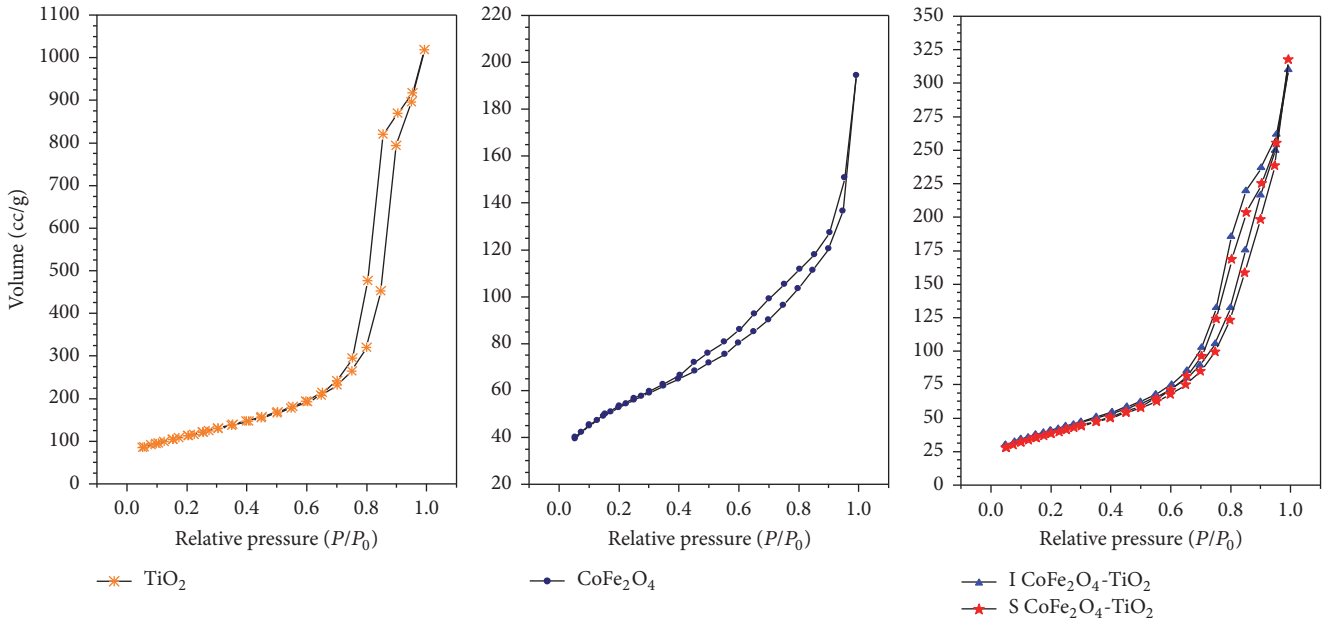

Figure 6: N_2 adsorption/desorption isotherms (at 77 K) of thermally treated samples: single $CoFe_2O_4$ and TiO_2 nanoparticles and hybrid $CoFe_2O_4$-TiO_2 nanoparticles. I: impregnation; S: seed.

Table 3: Textural properties (SA: surface area, PS: pore size, and PV: pore volume) of thermally treated samples: single $CoFe_2O_4$ and TiO_2 nanoparticles and hybrid $CoFe_2O_4$-TiO_2 nanoparticles. I: impregnation; S: seed.

Sample ID	SA (m^2/g)	PS (nm)	PV (cm^3/g)
TiO_2	403	14.8	1.6
$CoFe_2O_4$	184.9	1.4	0.293
I $CoFe_2O_4$-TiO_2	147.1	9.56	0.485
S $CoFe_2O_4$-TiO_2	138.6	9.58	0.497

In addition, it should be noted that the slight differences of the textural properties of hybrid $CoFe_2O_4$-TiO_2 nanoparticles can be related to the microemulsion synthesis approaches and therefore to the TiO_2 arrangement on cobalt ferrite phase supporting core. Obtained results confirm the capacity of the O/W microemulsion method to produce materials with good textural properties.

3.2.5. Magnetic Properties. Figure 7 shows the room-temperature magnetization versus applied field curves (M versus H) of thermally treated samples: cobalt ferrite NPs and hybrid $CoFe_2O_4$-TiO_2 nanoparticles, as well as the NPs physical mixture. Magnetization values are reported per gram of $CoFe_2O_4$, considering the 1 : 3 $CoFe_2O_4$-TiO_2 stablished molar ratio. First, it can be seen that the nanosized $CoFe_2O_4$ shows a typical ferrimagnetic hysteresis loop [52]; from the corresponding curve, the spinel ferrite displays a maximum magnetization (M_{max}) of 65 emu/g and a magnetic remanence (M_r) of 22 emu/g, with a coercitivity (H_c) of 1191 Oe. The obtained M_{max} value is lower than the reported value for the bulk counterpart (M_{max} 80 emu/g) [40, 53], but close to the range recorded for the $CoFe_2O_4$ nanoparticles (with

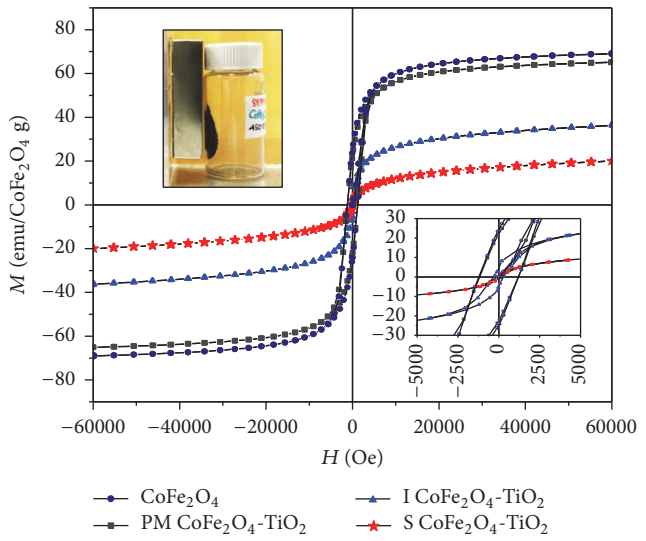

Figure 7: Magnetic hysteresis loops (at 300 K) of thermally treated samples: cobalt ferrite NPs; hybrid $CoFe_2O_4$-TiO_2 nanoparticles (impregnation and seed). NPs physical mixture (PM) is also reported.

average sizes of less than 50 nm), synthesized by water-in-oil microemulsions [42, 53] and even some other wet methods such as sol-gel [37], precipitation, and coprecipitation [36]. Besides, the obtained coercivity is also in the reported range. Second, compared with the curve of single $CoFe_2O_4$ NPS, the hybrid $CoFe_2O_4$-TiO_2 nanoparticles display a clearly different behavior, for instance, a very slim hysteresis loop (inset of Figure 7). The magnetic properties of the corresponding materials are summarized in Table 4; as it can be seen the M_{max} and M_r values are lower than those obtained from

Table 4: Magnetic properties (at 300 K) of thermally treated samples: cobalt ferrite NPs; hybrid $CoFe_2O_4$-TiO_2 nanoparticles (impregnation and seed). NPs physical mixture (PM) is also reported.

Sample ID	M_{max}	M_r	H_c (Oe)
$CoFe_2O_4$	65	22	1191
I $CoFe_2O_4$-TiO_2	18	5.82	289
S $CoFe_2O_4$-TiO_2	10	0.44	47.51
PM $CoFe_2O_4$-TiO_2	34	14	1228

bare $CoFe_2O_4$. The decrement on magnetic properties is a typical behavior of magnetic nanoparticles coated with titania nanocrystals, as reported in [18, 20, 21, 48]. This is attributed to the presence of nonmagnetic TiO_2 nanocrystals that act as a dead layer, breaking the long range order of the magnetic $CoFe_2O_4$ domains [54, 55]. Thus, it is possible to affirm that the hybrid $CoFe_2O_4$-TiO_2 NPs with weaker magnetic properties possess less magnetic dipole-dipole coupling, as a result of a more uniform titania wrapping on the cobalt ferrite surface. In this context, the seed microemulsion synthesis approach is a better option to develop a more efficient coating, in agreement with previous results (XRD and HRTEM-STEM). With the purpose of explaining the effect of the TiO_2 wrapping on cobalt ferrite surface, the $CoFe_2O_4$-TiO_2 NPs physical mixture magnetic curve is also presented. As can be seen, its hysteresis loop is almost overlapped with the $CoFe_2O_4$ NPs curve (Figure 7 inset), in contrast to the microemulsion synthesized hybrid $CoFe_2O_4$-TiO_2 nanoparticles. Therefore, the results coherently suggest that the $CoFe_2O_4$ magnetic domains in this sample are not disrupted, in contrast to the $CoFe_2O_4$ materials that are wrapped by the layer of TiO_2 nanocrystals, as in the synthesized $CoFe_2O_4$-TiO_2 hybrid nanomaterials, that presumably tend to behave like magnetic monodomains (especially the seed sample). The magnetic response shown by the impregnation and seed hybrid $CoFe_2O_4$-TiO_2 nanoparticles is attractive for magnetic recovery applications in heterogeneous photocatalysis. If a suitable magnetic field is applied near to the $CoFe_2O_4$-TiO_2 nanomaterials, the magnetic-photocatalytic nanocomposite powders could be easily collected, as shown in Figure 7. Furthermore, removal of the magnetic field would leave almost no residual magnetism on the hybrid nanoparticles, as a consequence of their low remanent magnetization; thus the powders could be redispersed for recycling, presumably without complications.

3.2.6. Surface Composition. To find out about chemical composition of obtained hybrid $CoFe_2O_4$-TiO_2 nanoparticles, X-ray photoelectron spectroscopy measurements were performed. Figure 8 shows the XPS spectra (Fe, Co, Ti, and O species) of the samples after thermal treatment. High-resolution XPS spectra for Fe 2p are presented on the first row. The Fe $2p^{3/2}$ main peak, shouldering with a satellite peak, is fitted into two signals, indicating the existence of Fe^{3+} species in two different lattice sites, as expected in a cubic spinel-type crystalline structure [52]. Each peak has associated a characteristic spin orbit splitting (doublet). For the impregnation sample, the binding energy at 709.6 eV arises from Fe^{3+} in octahedral sites ($Fe^{3+}{}_{OCT}$), while the binding energy at 710.99 eV is caused by Fe^{3+} in tetrahedral sites ($Fe^{3+}{}_{T}$). Similarly, in the seed sample, the two signals at 710.49 eV and 712.63 eV can be related to the octahedral and tetrahedral iron(III) [56, 57]. According to the integrated intensity of the fitted doublets, the distribution of Fe^{3+} in octahedral sites is 60% and 40% in tetrahedral sites. On the other hand (second row), the Co $2p^{3/2}$ XPS spectra of analyzed samples were fitted using three peaks; each peak has associated a characteristic spin orbit splitting (doublet) which leads to six-peak representation. First, for the impregnation sample, the binding energies at 779.07 and 780.90 eV are assigned to Co^{2+} ions in octahedral sites ($Co^{2+}{}_{OCT}$) and tetrahedral sites ($Co^{2+}{}_{T}$), respectively. Second, for the seed sample, the $Co^{2+}{}_{OCT}$ signal is situated at 781.32 eV and the $Co^{2+}{}_{T}$ signal on 784.58 eV. The ratio of Co^{2+} ions in octahedral to tetrahedral sites is obtained, from the integrated intensity of the fitted peaks, to be about 2 : 3. Additionally, the signals at 784.5 eV (I) and 788.09 (S) are characterized to be the satellite peak of Co $2p^{3/2}$ main line. Finally, corresponding XPS spectra for Ti2p and O1s signals are shown in the third and fourth rows. In the case of titanium, main $2p^{3/2}$ peak is observed at 457.498 eV (I) and 458.18 (S) with a spin orbit splitting of 5.86 eV and 5.73 eV, respectively; these peak positions were identified as that of Ti^{4+} from TiO_2. Binding energies slightly deviate from those reported for pure TiO_2 at 458.59 eV [58]. This could be an evidence of slight changes for right stoichiometry due to oxygen vacancies. Ti$2p^{3/2}$ peak was fitted with one peak in the case of the impregnation sample, which proves no other adsorbed species or additional phases; in the case of the seed approach sample, a second very low intensity peak can be identified (∗); this can be attributed to the Fe-O-Ti contribution, also inferred by XRD and UV-Vis results. With respect to oxygen, O1s peak is divided into three peaks. The main peak at 529.86 eV (I) and 529.89 eV (S) is attributed to the contribution of the crystal lattice oxygen (oxygen bonded to metal). However, the exact assignment of the two higher binding energy peaks is rather complex and controversial as numerous factors like surface defects, contaminants, impurities, or chemisorbed species could result in the appearance of the shoulder peaks. It is suggested that remaining contributions come from chemisorbed species like carbon (C-O) or hydrogen (O-H).

According to some studies, the architecture of core-shell type nanoparticles can be envisaged by XPS data interpretation [4, 59]. If $CoFe_2O_4$-TiO_2 hybrid nanoparticles are composed of a core-shell structure, the core signal would be partially or totally screened (as a function of layer thickness) by the signal of the corresponding shell. In this sense, Figure 9 displays the Fe $2p^{3/2}$ and Ti $2p^{3/2}$ detected peak intensities as a function of thermally treated hybrid nanoparticles. For the impregnation sample, the intensity of Fe signal is higher than the signal detected for titanium; in contrast, the Ti signal on the seed sample is by large above the iron signal. Therefore, it is coherent to assume that hybrid $CoFe_2O_4$-TiO_2 nanoparticles synthesized by the seed approach present a TiO_2 thicker layer over cobalt ferrite surface (or it is

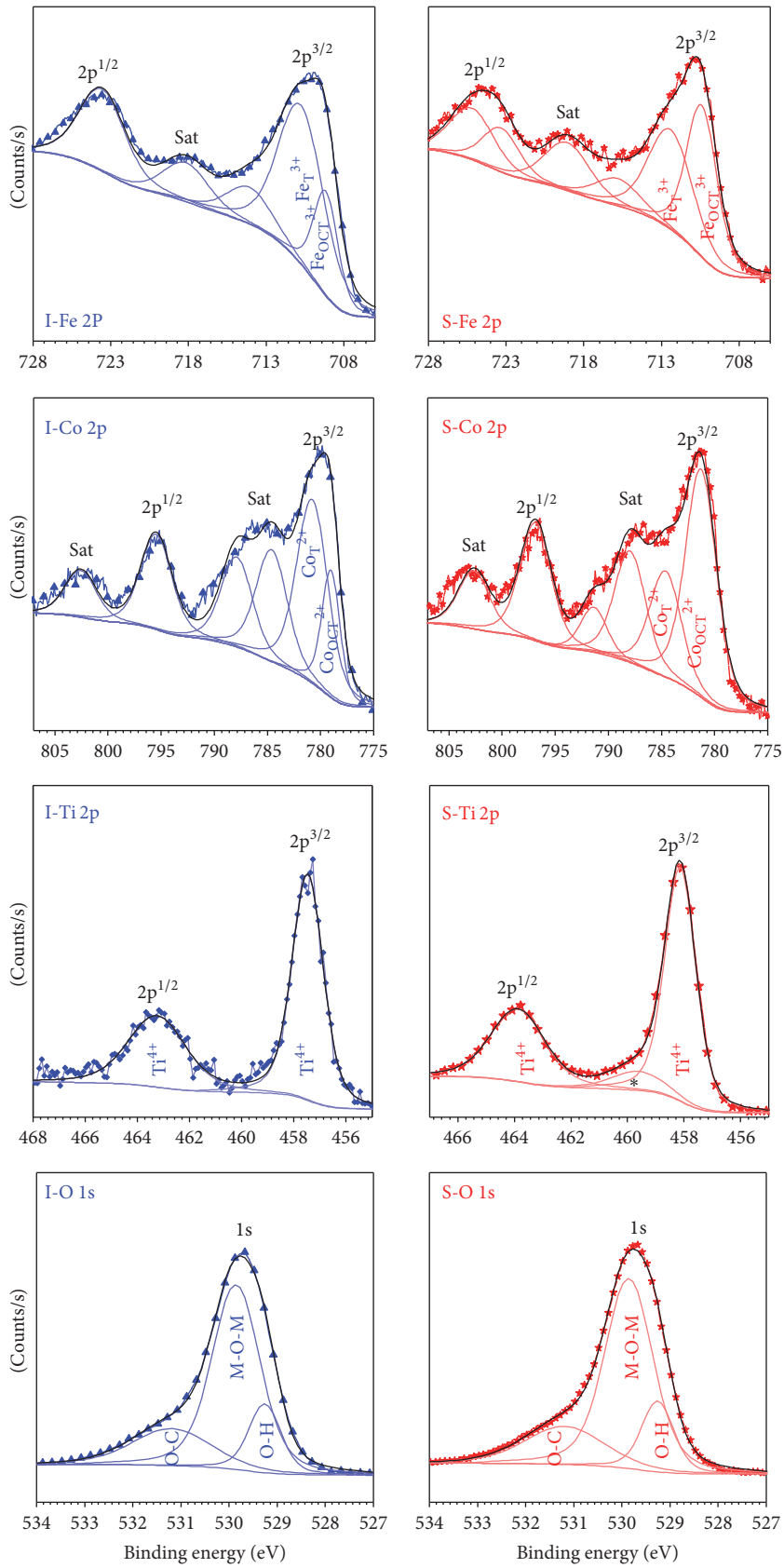

FIGURE 8: XPS spectra (Fe, Co, Ti, and O species) for $CoFe_2O_4$-TiO_2 thermally treated hybrid nanoparticles synthesized by the (I) impregnation and (S) seed approaches.

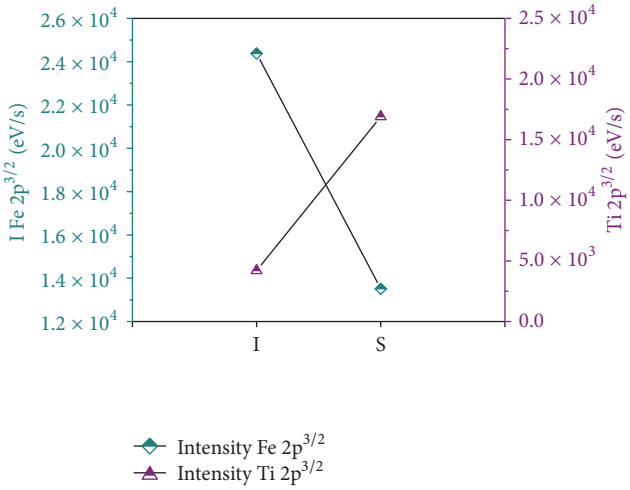

FIGURE 9: Fe $2p^{3/2}$ and Ti $2p^{3/2}$ XPS intensity signals in function of the thermally treated hybrid $CoFe_2O_4$-TiO_2 nanoparticles synthesized by the (I) impregnation and (S) seed approaches.

more uniformly coated) in comparison with the hybrid nanoparticles synthesized by the impregnation approach.

4. Conclusions

$CoFe_2O_4$-TiO_2 hybrid nanoparticles were successfully prepared by the impregnation and seed approaches, based on the oil-in-water microemulsion reaction method conditions of single $CoFe_2O_4$ and TiO_2 nanoparticles. Applied thermal treatment allowed the crystallization of anatase TiO_2 NPs layer within the cubic spinel-type $CoFe_2O_4$ nanoparticles, for both synthesis cases, as demonstrated by XRD patterns; the shape and intensity of main diffraction signals suggested differences on $CoFe_2O_4$-TiO_2 heterostructures, due to the arrangement of TiO_2 onto the cobalt ferrite phase, as confirmed by electron microscopy images, which depicted partial decoration, for the impregnation approach, and a more uniform coverage (core-shell like), for the seed approach. In the same way, the elemental mapping of seed-mediated sample exhibited a homogeneous titanium distribution in contrast to the impregnation approach; however a well-defined $CoFe_2O_4$-TiO_2 chemical composition was obtained for the two developed approaches, as proved by atomic absorption spectroscopy and EDX microanalysis. The study of optical properties showed the ultraviolet and visible light absorption capability of hybrid nanoparticles, as a consequence of bandgap energies modification, due to cobalt ferrite and titanium oxide coupling. The assessed textural properties exposed the high surface areas of $CoFe_2O_4$-TiO_2 hybrid nanomaterials (as well as single phase nanoparticles); the integration of titanium oxide within $CoFe_2O_4$ phase resulted in a major gas absorption capability, as indicated by the obtained adsorption/desorption isotherms. $CoFe_2O_4$ magnetic properties were clearly altered with the attaching of nonmagnetic TiO_2 layer; thus it was possible to assume that the hybrid nanoparticles synthesized by the seed approach possessed a much more continuous coverage coating due to the apparently magnetic monodomain behavior displayed by the corresponding magnetic curve. XPS analysis shows the presence of Fe^{3+}, Co^{2+} ($CoFe_2O_4$ phase), and Ti^{4+} (TiO_2 phase) chemical states on the surface of synthesized and thermally treated samples, and the titanium peak intensities suggested its predominance over $CoFe_2O_4$ nanoparticles surface, especially for the seed approach. In addition, the characterization of the $CoFe_2O_4$-TiO_2 NPs physical mixture provided enough evidence of the characteristics possessed by a hybrid nanomaterial with a poor interaction between its components, in comparison with the microemulsion synthesized hybrid nanomaterials. In summary, this report provides new microemulsion synthesis strategies for the straightforward design of $CoFe_2O_4$-TiO_2 hybrid nanoparticles. The characteristics of synthesized hybrid nanoparticles are suitable for potential applications in the field of photocatalysis.

Competing Interests

The authors declare that there is no conflict of interests regarding the publication of this paper.

Acknowledgments

The authors are grateful to CONACYT (CB Project Grant no. CB2011/166649 and Proyecto Redes Temáticas no. 194451). The authors also acknowledge Aleyda Cavazos Cavazos (CIMAV Monterrey), Luis G. Silva Vidaurri (CIMAV Monterrey), Luis de la Torre Sáenz (CIMAV Chihuahua), Gilberto H. López (CIQA), Omar Ali Carrasco Jaim (UANL), and Dr. Isaías Juárez Ramírez (UANL) for their help with atomic absorption spectroscopy, XPS BET, VSM, and UV-Vis measurements, respectively.

References

[1] P. M. Ajayan, "Bulk metal and ceramics nanocomposites," in *Nanocomposite Science and Technology*, pp. 1–75, Wiley-VCH, 2004.

[2] R. Marschall, "Semiconductor composites: strategies for enhancing charge carrier separation to improve photocatalytic activity," *Advanced Functional Materials*, vol. 24, no. 17, pp. 2421–2440, 2014.

[3] Y. L. Pang, S. Lim, H. C. Ong, and W. T. Chong, "Research progress on iron oxide-based magnetic materials: synthesis techniques and photocatalytic applications," *Ceramics International*, vol. 42, no. 1, 2015.

[4] M. Stefan, O. Pana, C. Leostean et al., "Synthesis and characterization of Fe_3O_4–TiO_2 core-shell nanoparticles," *Journal of Applied Physics*, vol. 116, no. 11, Article ID 114312, 2014.

[5] S. Bhaduri and S. B. Bhaduri, "Recent developments in ceramic nanocomposites," *JOM*, vol. 50, no. 1, pp. 44–51, 1998.

[6] P. Palmero, "Structural ceramic nanocomposites: a review of properties and powders' synthesis methods," *Nanomaterials*, vol. 5, no. 2, pp. 656–696, 2015.

[7] M. Dahl, Y. Liu, and Y. Yin, "Composite titanium dioxide nanomaterials," *Chemical Reviews*, vol. 114, no. 19, pp. 9853–9889, 2014.

[8] S. Xuan, W. Jiang, X. Gong, Y. Hu, and Z. Chen, "Magnetically separable Fe_3O_4/TiO_2 hollow spheres: fabrication and photocatalytic activity," *Journal of Physical Chemistry C*, vol. 113, no. 2, pp. 553–558, 2009.

[9] H. Yao, M. Fan, Y. Wang, G. Luo, and W. Fei, "Magnetic titanium dioxide based nanomaterials: synthesis, characteristics, and photocatalytic application in pollutant degradation," *Journal of Materials Chemistry A*, vol. 3, no. 34, pp. 17511–17524, 2015.

[10] F. Fresno, R. Portela, S. Suárez, and J. M. Coronado, "Photocatalytic materials: recent achievements and near future trends," *Journal of Materials Chemistry A*, vol. 2, no. 9, pp. 2863–2884, 2014.

[11] H. Xu, S. Ouyang, L. Liu, P. Reunchan, N. Umezawa, and J. Ye, "Recent advances in TiO_2-based photocatalysis," *Journal of Materials Chemistry A*, vol. 2, no. 32, pp. 12642–12661, 2014.

[12] Y. Yao, J. Qin, H. Chen et al., "One-pot approach for synthesis of N-doped TiO2/ZnFe2O4 hybrid as an efficient photocatalyst for degradation of aqueous organic pollutants," *Journal of Hazardous Materials*, vol. 291, pp. 28–37, 2015.

[13] H. Liu, Y. He, and X. Liang, "Magnetic photocatalysts containing TiO_2 nanocrystals: morphology effect on photocatalytic activity," *Journal of Materials Research*, vol. 29, no. 1, pp. 98–106, 2014.

[14] S. Rana, R. S. Srivastava, M. M. Sorensson, and R. D. K. Misra, "Synthesis and characterization of nanoparticles with magnetic core and photocatalytic shell: anatase TiO_2-$NiFe_2O_4$ system," *Materials Science and Engineering B: Solid-State Materials for Advanced Technology*, vol. 119, no. 2, pp. 144–151, 2005.

[15] G.-Y. Zhang, Y.-Q. Sun, D.-Z. Gao, and Y.-Y. Xu, "Quasi-cube $ZnFe_2O_4$ nanocrystals: hydrothermal synthesis and photocatalytic activity with TiO_2 (Degussa P25) as nanocomposite," *Materials Research Bulletin*, vol. 45, no. 7, pp. 755–760, 2010.

[16] H. Li, Y. Zhang, S. Wang, Q. Wu, and C. Liu, "Study on nanomagnets supported TiO_2 photocatalysts prepared by a sol-gel process in reverse microemulsion combining with solvent-thermal technique," *Journal of Hazardous Materials*, vol. 169, no. 1–3, pp. 1045–1053, 2009.

[17] H. A. J. L. Mourão, A. R. Malagutti, and C. Ribeiro, "Synthesis of TiO_2-coated $CoFe_2O_4$ photocatalysts applied to the photodegradation of atrazine and rhodamine B in water," *Applied Catalysis A: General*, vol. 382, no. 2, pp. 284–292, 2010.

[18] P. Sathishkumar, R. V. Mangalaraja, S. Anandan, and M. Ashokkumar, "$CoFe_2O_4/TiO_2$ nanocatalysts for the photocatalytic degradation of Reactive Red 120 in aqueous solutions in the presence and absence of electron acceptors," *Chemical Engineering Journal*, vol. 220, pp. 302–310, 2013.

[19] P. Pongwan, B. Inceesungvorn, S. Phanichphant, W. Kangwansupamonkon, and N. Wetchakun, "Synthesis and characterization of a magnetically separable $CoFe_2O_4/TiO_2$ nanocomposite for the photomineralization of formic acid," *Ferroelectrics*, vol. 453, no. 1, pp. 133–140, 2013.

[20] C. Haw, W. Chiu, S. Abdul Rahman et al., "The design of new magnetic-photocatalyst nanocomposites ($CoFe_2O_4$-TiO_2) as smart nanomaterials for recyclable-photocatalysis applications," *New Journal of Chemistry*, vol. 40, no. 2, pp. 1124–1136, 2016.

[21] W. Fu, H. Yang, M. Li, M. Li, N. Yang, and G. Zou, "Anatase TiO_2 nanolayer coating on cobalt ferrite nanoparticles for magnetic photocatalyst," *Materials Letters*, vol. 59, no. 27, pp. 3530–3534, 2005.

[22] S. M. Moosavi, P. Molla-Abbasi, and Z. Haji-Aghajani, "Photocatalyst $CoFe_2O_4$–TiO_2: application in photo-degradation of organic dyes and magnetic nanocomposite preparation," *Journal of Materials Science: Materials in Electronics*, vol. 27, no. 5, pp. 4879–4886, 2016.

[23] M. Sanchez-Dominguez, M. Boutonnet, and C. Solans, "A novel approach to metal and metal oxide nanoparticle synthesis: the oil-in-water microemulsion reaction method," *Journal of Nanoparticle Research*, vol. 11, no. 7, pp. 1823–1829, 2009.

[24] M. Sanchez-Dominguez, K. Pemartin, and M. Boutonnet, "Preparation of inorganic nanoparticles in oil-in-water microemulsions: a soft and versatile approach," *Current Opinion in Colloid & Interface Science*, vol. 17, no. 5, pp. 297–305, 2012.

[25] M. Boutonnet, J. Kizling, P. Stenius, and G. Maire, "The preparation of monodisperse colloidal metal particles from microemulsions," *Colloids and Surfaces*, vol. 5, no. 3, pp. 209–225, 1982.

[26] K. Pemartin, C. Solans, G. Vidal-Lopez, and M. Sanchez-Dominguez, "Synthesis of ZnO and ZnO_2 nanoparticles by the oil-in-water microemulsion reaction method," *Chemistry Letters*, vol. 41, no. 10, pp. 1032–1034, 2012.

[27] M. Sanchez-Dominguez, L. F. Liotta, G. Di Carlo et al., "Synthesis of CeO_2, ZrO_2, $Ce_{0.5}Zr_{0.5}O_2$, and TiO_2 nanoparticles by a novel oil-in-water microemulsion reaction method and their use as catalyst support for CO oxidation," *Catalysis Today*, vol. 158, no. 1-2, pp. 35–43, 2010.

[28] C. Tiseanu, V. I. Parvulescu, M. Boutonnet et al., "Surface versus volume effects in luminescent ceria nanocrystals synthesized by an oil-in-water microemulsion method," *Physical Chemistry Chemical Physics*, vol. 13, no. 38, pp. 17135–17145, 2011.

[29] G. Di Carlo, M. Lualdi, A. M. Venezia, M. Boutonnet, and M. Sanchez-Dominguez, "Design of cobalt nanoparticles with tailored structural and morphological properties via O/W and W/O microemulsions and their deposition onto silica," *Catalysts*, vol. 5, no. 1, pp. 442–459, 2015.

[30] M. Sanchez-Dominguez, H. Koleilat, M. Boutonnet, and C. Solans, "Synthesis of pt nanoparticles in oil-in-water microemulsions: phase behavior and effect of formulation parameters on nanoparticle characteristics," *Journal of Dispersion Science and Technology*, vol. 32, no. 12, pp. 1765–1770, 2011.

[31] M. Sanchez-Dominguez, G. Morales-Mendoza, M. J. Rodriguez-Vargas et al., "Synthesis of Zn-doped TiO_2 nanoparticles by the novel oil-in-water (O/W) microemulsion method and their use for the photocatalytic degradation of phenol," *Journal of Environmental Chemical Engineering*, vol. 3, no. 4, pp. 3037–3047, 2015.

[32] K. Pemartin-Biernath, A. V. Vela-González, M. B. Moreno-Trejo et al., "Synthesis of mixed Cu/Ce oxide nanoparticles by the oil-in-water microemulsion reaction method," *Materials*, vol. 9, no. 6, article 480, 2016.

[33] K. Pemartin, C. Solans, J. Alvarez-Quintana, and M. Sanchez-Dominguez, "Synthesis of Mn–Zn ferrite nanoparticles by the oil-in-water microemulsion reaction method," *Colloids and Surfaces A: Physicochemical and Engineering Aspects*, vol. 451, no. 1, pp. 161–171, 2014.

[34] C. Okoli, M. Sanchez-Dominguez, M. Boutonnet et al., "Comparison and functionalization study of microemulsion-prepared magnetic iron oxide nanoparticles," *Langmuir*, vol. 28, no. 22, pp. 8479–8485, 2012.

[35] E. Swatsitang, S. Phokha, S. Hunpratub et al., "Characterization and magnetic properties of cobalt ferrite nanoparticles," *Journal of Alloys and Compounds*, vol. 664, pp. 792–797, 2016.

[36] M. Houshiar, F. Zebhi, Z. J. Razi, A. Alidoust, and Z. Askari, "Synthesis of cobalt ferrite ($CoFe_2O_4$) nanoparticles using

combustion, coprecipitation, and precipitation methods: A comparison study of size, structural, and magnetic properties," *Journal of Magnetism and Magnetic Materials*, vol. 371, pp. 43–48, 2014.

[37] M. Sajjia, M. Oubaha, M. Hasanuzzaman, and A. G. Olabi, "Developments of cobalt ferrite nanoparticles prepared by the sol-gel process," *Ceramics International*, vol. 40, no. 1, pp. 1147–1154, 2014.

[38] V. V. Paike, P. S. Niphadkar, V. V. Bokade, and P. N. Joshi, "Synthesis of spinel $CoFe_2O_4$ via the Co-precipitation method using tetraalkyl ammonium hydroxides as precipitating agents," *Journal of the American Ceramic Society*, vol. 90, no. 9, pp. 3009–3012, 2007.

[39] P. D. Thang, G. Rijnders, and D. H. A. Blank, "Spinel cobalt ferrite by complexometric synthesis," *Journal of Magnetism and Magnetic Materials*, vol. 295, no. 3, pp. 251–256, 2005.

[40] S. M. Montemayor, L. A. García-Cerda, and J. R. Torres-Lubián, "Preparation and characterization of cobalt ferrite by the polymerized complex method," *Materials Letters*, vol. 59, no. 8-9, pp. 1056–1060, 2005.

[41] S. Rana, J. Philip, and B. Raj, "Micelle based synthesis of cobalt ferrite nanoparticles and its characterization using Fourier Transform Infrared Transmission Spectrometry and Thermogravimetry," *Materials Chemistry and Physics*, vol. 124, no. 1, pp. 264–269, 2010.

[42] V. Pillai and D. O. Shah, "Synthesis of high-coercivity cobalt ferrite particles using water-in-oil microemulsions," *Journal of Magnetism and Magnetic Materials*, vol. 163, no. 1-2, pp. 243–248, 1996.

[43] A. Ajmal, I. Majeed, R. N. Malik, H. Idriss, and M. A. Nadeem, "Principles and mechanisms of photocatalytic dye degradation on TiO_2 based photocatalysts: a comparative overview," *RSC Advances*, vol. 4, no. 70, pp. 37003–37026, 2014.

[44] E. Masolo, N. Senes, E. Pellicer et al., "Evaluation of the anatase/rutile phase composition influence on the photocatalytic performances of mesoporous TiO_2 powders," *International Journal of Hydrogen Energy*, vol. 40, no. 42, pp. 14483–14491, 2015.

[45] M. Abbas, B. P. Rao, V. Reddy, and C. Kim, "Fe_3O_4/TiO_2 core/shell nanocubes: single-batch surfactantless synthesis, characterization and efficient catalysts for methylene blue degradation," *Ceramics International*, vol. 40, no. 7, pp. 11177–11186, 2014.

[46] P. Raju and S. R. Murthy, "Microwave-hydrothermal synthesis of $CoFe_2O_4$-TiO_2 nanocomposites," *Advanced Materials Letters*, vol. 4, no. 1, pp. 99–105, 2013.

[47] Y. Gao, B. Chen, H. Li, and Y. Ma, "Preparation and characterization of a magnetically separated photocatalyst and its catalytic properties," *Materials Chemistry and Physics*, vol. 80, no. 1, pp. 348–355, 2003.

[48] C.-J. Li, J.-N. Wang, B. Wang, J. R. Gong, and Z. Lin, "Direct formation of reusable $TiO_2/CoFe_2O_4$ heterogeneous photocatalytic fibers via two-spinneret electrospinning," *Journal of Nanoscience and Nanotechnology*, vol. 12, no. 3, pp. 2496–2502, 2012.

[49] S. Liu, W. Wang, J. Chen et al., "Foamed single-crystalline anatase nanocrystals exhibiting enhanced photocatalytic activity," *Journal of Materials Chemistry A*, vol. 3, no. 34, pp. 17837–17848, 2015.

[50] R. Ren, Z. Wen, S. Cui, Y. Hou, X. Guo, and J. Chen, "Controllable synthesis and tunable photocatalytic properties of Ti^{3+}-doped TiO_2," *Scientific Reports*, vol. 5, article 10714, 2015.

[51] M. A. Nazarkovsky, V. M. Bogatyrov, B. Czech et al., "Titania-coated nanosilica-cobalt ferrite composites: structure and photocatalytic activity," *Journal of Photochemistry and Photobiology A: Chemistry*, vol. 319-320, pp. 40–52, 2016.

[52] R. Valenzuela, *Magnetic Ceramics*, Cambridge University Press, 1994.

[53] P. Puliová, J. Kováč, A. Voigt, and P. Raschman, "Structure and magnetic properties of Co and Ni nano-ferrites prepared by a two step direct microemulsions synthesis," *Journal of Magnetism and Magnetic Materials*, vol. 341, pp. 93–99, 2013.

[54] H. Hamad, M. Abd El-Latif, A. E.-H. Kashyout, W. Sadik, and M. Feteha, "Synthesis and characterization of core-shell-shell magnetic ($CoFe_2O_4$-SiO_2-TiO_2) nanocomposites and TiO_2 nanoparticles for the evaluation of photocatalytic activity under UV and visible irradiation," *New Journal of Chemistry*, vol. 39, no. 4, pp. 3116–3128, 2015.

[55] F. A. Harraz, R. M. Mohamed, M. M. Rashad, Y. C. Wang, and W. Sigmund, "Magnetic nanocomposite based on titania–silica/cobalt ferrite for photocatalytic degradation of methylene blue dye," *Ceramics International*, vol. 40, no. 1, pp. 375–384, 2014.

[56] W. P. Wang, H. Yang, T. Xian, and J. L. Jiang, "XPS and magnetic properties of $CoFe_2O_4$ nanoparticles synthesized by a polyacrylamide gel route," *Materials Transactions*, vol. 53, no. 9, pp. 1586–1589, 2012.

[57] M. C. Biesinger, B. P. Payne, A. P. Grosvenor, L. W. M. Lau, A. R. Gerson, and R. S. C. Smart, "Resolving surface chemical states in XPS analysis of first row transition metals, oxides and hydroxides: Cr, Mn, Fe, Co and Ni," *Applied Surface Science*, vol. 257, no. 7, pp. 2717–2730, 2011.

[58] M. C. Biesinger, L. W. M. Lau, A. R. Gerson, and R. S. C. Smart, "Resolving surface chemical states in XPS analysis of first row transition metals, oxides and hydroxides: Sc, Ti, V, Cu and Zn," *Applied Surface Science*, vol. 257, no. 3, pp. 887–898, 2010.

[59] W. Wu, X. Xiao, S. Zhang, F. Ren, and C. Jiang, "Facile method to synthesize magnetic iron oxides/TiO_2 hybrid nanoparticles and their photodegradation application of methylene blue," *Nanoscale Research Letters*, vol. 6, article 533, 2011.